AIAA JOURNAL
Vol. 44, No. 3, March 2006

Parametric Studies of Aluminum Combustion Model for Simulations of Detonation Waves

Krzysztof Benkiewicz* and A. Koichi Hayashi†
Aoyama Gakuin University, Kanagawa 229-8558, Japan

We present a parametric analysis of a combustion model developed for computer simulations of detonation waves propagating in aluminum-dust–oxygen two-phase mixtures. In this model, consumption of solid and liquid aluminum is limited by its evaporation rate, and, depending on a gas-phase temperature, the fuel can be burned into aluminum oxide or aluminum monoxide. The model is applied for one-dimensional simulations of detonation waves. We analyze the influence of various factors on characteristic parameters of the detonation and compare computed results with those of other models and experimental data. The analyses show a qualitative agreement of the computed results with the Chapman–Jouguet detonation model. A combustion model and an initial solid-phase concentration significantly influence the computed solutions. Specifically, a decomposition temperature has a strong effect on the system, because it limits the energy release in the combustion process. An initial particle diameter (with an exception of very fine dust) and an ignition temperature have no influence on the propagation of the detonation waves but are limiting factors for their development.

Nomenclature

B	=	universal gas constant
C_{pk}	=	kth species specific heat at constant pressure ($k = 1, \ldots, n_s$)
C_{vs}	=	solid-phase specific heat
C_x	=	drag force coefficient
c_s	=	solid-phase concentration
D	=	detonation wave velocity
D_{CJ}	=	Chapman–Jouguet detonation wave velocity
d	=	average particle diameter
d_0	=	initial particle diameter
E_l	=	lth phase total specific energy (thermal and kinetic)
e_l	=	lth phase specific internal energy (thermal) ($l = g, s$, where g is gas and s is solid)
$\boldsymbol{F}$	=	vector of fluxes
f	=	particle breakup (agglomeration) rate, 1/s
h	=	interphase heat transfer factor $\mathrm{kg/s^3 \cdot m \cdot K}$
h_{f298g_k}	=	kth species heat of formation
h_{f298s}	=	solid-phase heat of formation
K_r	=	combustion rate constant, $\mathrm{s/m^2}$
Ma	=	Mach number
M_g	=	average molar mass of gaseous mixture
N_p	=	particle number density, $1/\mathrm{m^3}$
Nu	=	Nusselt number
n_s	=	species number
p_{CJ}	=	Chapman–Jouguet detonation pressure
p_g	=	gas pressure
p_{vN}	=	peak pressure (von Neumann spike)
Re	=	Reynolds number
$\boldsymbol{S}$	=	vector of source terms
T_{dec}	=	aluminum oxide decomposition temperature
T_{ign}	=	ignition temperature
T_l	=	lth phase temperature
t	=	time coordinate
$\boldsymbol{U}$	=	vector of variables
u_l	=	lth phase velocity component
x	=	spatial coordinate (direction)
Y_k	=	kth gaseous species mass fraction
Δc	=	interphase mass exchange factor, $\mathrm{kg/s \cdot m^3}$
Δc_k	=	kth species interphase mass exchange factor, $\mathrm{kg/s \cdot m^3}$
δ	=	interphase drag force factor, $\mathrm{kg/s \cdot m^3}$
λ_g	=	gas-phase heat conduction coefficient
π	=	3.1415927 . . .
ρ_{g_k}	=	kth species partial density
ρ_l	=	lth phase material density
τ	=	characteristic combustion time
ϕ_s	=	solid-phase volume fraction
$\dot{\omega}_k$	=	kth species production (consumption) rate due to homogeneous chemical reactions

Subscripts

CJ	=	Chapman–Jouguet point
g	=	gas phase
k	=	gaseous species index
l	=	phase index
s	=	solid phase
vN	=	von Neumann spike

Introduction

THE hazard of dust detonations has been an inherent part of our industrial activity from the beginning of the Industrial Age. Combustible dust is present in industrial facilities as the product or side effect of many technological processes. In certain cases a mixture of gas and solid particles or liquid droplets created during, e.g., pneumatic transport of various materials can detonate and show its destructive power. Even though the structure and mechanism of propagation of the detonation waves in various media have been analyzed experimentally and theoretically by many scientists, dust explosions still threaten contemporary industry.

Fine aluminum dust is often used as an energetic and stabilizing ingredient of solid-fuel propellants, but its production is associated with certain hazards for human beings and industrial facilities. Although aluminum dust is difficult to ignite, it can detonate and cause loss of life and serious damage to powder processing plants (see, e.g., Eckhoff[1] for examples). Then, it is very important

Received 2 September 2002; accepted for publication 15 September 2005.

*Graduate Student, Department of Mechanical Engineering, 5-10-1 Fuchinobe, Sagamihara.

†Professor, Department of Mechanical Engineering, 5-10-1 Fuchinobe, Sagamihara.

to study aluminum-dust detonations to improve the safety of such facilities.

The detonation of aluminum dust has been studied experimentally by many researchers. Strauss[2] conducted shock-tube experiments of the detonation of aluminum dust suspended in an atmosphere of oxygen. Tulis and Selman[3] and Borisov et al.[4] used the same technique to study the detonation of aluminum powder dispersed in air. These works were concentrated on basic properties of the detonation waves, i.e., on an evaluation of the detonation wave velocity, peak pressures, and detonability limits. Zhang et al.[5] studied the deflagration-to-detonation transition (DDT) in aluminum dust–air mixtures and showed that the propagation of steady self-sustained detonation waves in such mixtures may require shock-tube diameters larger than 0.1 m and length–diameter ratios higher than 100. Tulis,[6] Tulis and Selman,[7] and Ingignoli et al.[8] showed the possibility of an unconfined detonation of mixtures containing aluminum particles in suspension in air and in oxygen, although such experiments required the application of very fine dust, near-stoichiometric dust concentrations, large dust clouds, and very strong initiations.

An interesting group of problems is the detonation of hybrid systems, i.e., mixtures of combustible gases and aluminum particles. Such systems have been investigated, e.g., by Zhang et al.,[9] Veyssiére,[10,11] Veyssiére et al.,[12] and Ingignoli.[13] In the latter three references it was observed that a supersonic combustion wave can propagate as a pseudo-gas detonation (PGD), single-front detonation (SFD), or double-front detonation (DFD).

The detonation of aluminum dust suspended in various oxidizing atmospheres has also been studied numerically. Interesting results were presented, e.g., by Borisov et al.,[4] Fedorov et al.,[14] and Ingignoli.[13] Khasainov and Veyssiére,[15,16] Veyssiére and Khasainov,[17,18] and Ingignoli[13] investigated the detonation in hybrid mixtures and confirmed that, depending on fuel concentration, the detonation wave can propagate in three different regimes.

An important problem in the application of numerical simulations is related to many parameters and coefficients that define the physics of the process. Some of them are not known at all, others are difficult to measure, and many others are only estimated with some amount of uncertainty. We have to understand their influence on the computed results. In such analyses, often called "parametric studies," we vary one of many factors and observe changes of the most important parameters of the process.

In this paper, we will conduct parametric studies of an aluminum-dust combustion model. We will apply it to numerical simulations of initiation and propagation of the detonation waves in two-phase mixtures consisting of aluminum particles suspended in an atmosphere of pure oxygen. Our aim is to analyze the influence of various parameters on the computed solutions, to develop a practical aluminum-dust combustion model, and to understand its limitations. We will also compare the computed results with those of other theoretical models and experimental data accessible in the literature.

Mathematical Formulation

Let us consider a mixture consisting of small, spherical, solid particles suspended in a multicomponent gaseous atmosphere. Assume that the mixture is dilute and that particle–particle collisions are negligible. Suppose also that the number of particles is large enough to allow for the application of a continuum hypothesis to the condensed phase. In such a situation, we can treat both phases as two interpenetrating continua that can be in thermal and mechanical nonequilibrium. Their motion can be described by using modified Euler equations, in which phase interactions are represented by source terms. If we consider a one-dimensional geometry, then the system of equations in a vector form can be written as

$$\frac{\partial \boldsymbol{U}}{\partial t} + \frac{\partial \boldsymbol{F}}{\partial x} = \boldsymbol{S} \tag{1}$$

where the vectors of variables $\boldsymbol{U}$, fluxes $\boldsymbol{F}$, and source terms $\boldsymbol{S}$ are defined as

$$\boldsymbol{U} = \begin{bmatrix} \rho_{g_k} \\ \rho_g \\ \rho_g u_g \\ \rho_g E_g \\ \phi_s \rho_s \\ \phi_s \rho_s u_s \\ \phi_s \rho_s E_s \\ N_p \end{bmatrix}, \qquad \boldsymbol{F} = \begin{bmatrix} \rho_{g_k} u_g \\ \rho_g u_g \\ \rho_g u_g^2 + p_g \\ (\rho_g E_g + p_g) u_g \\ \phi_s \rho_s u_s \\ \phi_s \rho_s u_s^2 \\ \phi_s \rho_s E_s u_s \\ N_p u_s \end{bmatrix} \tag{2}$$

$$\boldsymbol{S} = \begin{bmatrix} \dfrac{1}{1-\phi_s}\left[\Delta c_k\left(1-\dfrac{\rho_g}{\rho_s}\right)\right] + \dot{\omega}_k \\ \dfrac{1}{1-\phi_s}\left[\Delta c\left(1-\dfrac{\rho_g}{\rho_s}\right)\right] \\ \dfrac{1}{1-\phi_s}\left[\left(\dfrac{\Delta c}{2}-\delta\right)(u_g-u_s) + \Delta c\left(u_s - u_g\dfrac{\rho_g}{\rho_s}\right)\right] \\ \dfrac{\left(\dfrac{\Delta c}{2}-\delta\right)(u_g-u_s)u_s + \Delta c\left(E_s - E_g\dfrac{\rho_g}{\rho_s}\right) - h(T_g-T_s)}{1-\phi_s} \\ -\Delta c \\ -\left(\dfrac{\Delta c}{2}-\delta\right)(u_g-u_s) - \Delta c u_s \\ -\left(\dfrac{\Delta c}{2}-\delta\right)(u_g-u_s)u_s - \Delta c E_s + h(T_g-T_s) \\ f \end{bmatrix} \tag{3}$$

The terms ρ_l, u_l, T_l, and E_l are the lth phase ($l = g, s$) material density, velocity, temperature, and total (internal and kinetic) specific energy, respectively. The latter is defined as

$$E_l = e_l + u_l^2/2 \tag{4}$$

where e_l is a specific internal (thermal and chemical) energy of the lth phase. For the gas phase it is computed from

$$e_g(T_g) = \sum_{k=1}^{n_s}\left\{Y_k\left[h_{f298_{g_k}} + \int_{298}^{T_g} C_{pk}(T)\,\mathrm{d}T\right]\right\} - \frac{B}{M_g}T_g \tag{5}$$

n_s is a number of components in the gaseous mixture and Y_k, $h_{f298_{g_k}}$, and C_{pk} are the kth species ($k = 1, \ldots, n_s$) mass fraction, enthalpy of formation at 298.15 K, and specific heat at constant pressure, respectively. The latter is a polynomial function of the gas-phase temperature T_g. B is an universal gas constant, and M_g is a molar mass of the gaseous mixture. The specific internal energy of the solid phase is defined as

$$e_s(T_s) = h_{f298_s} + \int_{298}^{T_s} C_{vs}(T)\,\mathrm{d}T \tag{6}$$

where h_{f298_s} is the solid-phase enthalpy of formation at 298.15 K. C_{vs} is the solid-phase specific heat at constant volume. It is a function of the solid-phase temperature T_s and already includes all of the phase transitions. The model considered here takes into account a pressure correction for a solid-phase boiling temperature. A gas-phase pressure is obtained from

$$p_g = \rho_g (B/M_g) T_g \tag{7}$$

The terms ρ_{g_k} and $\dot{\omega}_k$ in Eqs. (2) and (3) are the kth species partial density and source term due to homogeneous chemical reactions (if

present in the system). N_p is a particle number density (number of particles per unit volume), ϕ_s is a solid-phase volume fraction (the ratio of a volume occupied by particles and a total volume of the system), and f is a particle breakup (source) or coalescence (sink) rate.

The phase interactions can involve an exchange of mass, momentum, and energy between the gas and the condensed phase. Δc is an interphase mass transfer (total), whereas Δc_k is its partial contribution to the kth gaseous species. These terms are defined by a combustion model described in the next section. The exchange of the momentum between both phases can occur due to a velocity difference between the gas and particles and due to the interphase mass transfer. The former is a drag force represented by an interphase drag-force factor δ, which can be obtained from

$$\delta = \tfrac{3}{4}(\phi_s/d)C_x\rho_g|u_g - u_s| \tag{8}$$

The drag force coefficient C_x is a function of Reynolds and Mach numbers and is computed by using a formula proposed by Henderson.[19] The energy exchange between the phases can take place due to mass transfer, work done by drag forces, and heat transfer between the phases. The latter is represented by an interphase heat transfer factor h, which can be computed from

$$h = 6\phi_s\left(Nu\lambda_g\big/d^2\right) \tag{9}$$

Nu is a Nusselt number calculated from equations derived by Carlson and Hoglund.[20] The gas-phase heat conduction coefficient (λ_g) and viscosity are computed by using formulas described in Kee et al.[21]

As one can notice, Eqs. (8) and (9) depend on the particle diameter d. Here we are interested in an average diameter of particles or, in other words, we are looking for equivalent particles that are locally uniform in size and represent a real dust. The average particle diameter is then computed from the following geometrical relationship between the particle number density N_p and the condensed-phase volume fraction ϕ_s:

$$d = (6\phi_s/\pi N_p)^{\frac{1}{3}} \tag{10}$$

In Eqs. (1–3) the total mass of the mixture is conserved, but the formulation used here is slightly more complicated than systems of equations usually presented in the literature on two-phase flows. To separate and simplify the solution of the homogeneous parts of the gas- and solid-phase equations, we have ruled out a gas-phase volume fraction ($\phi_g = 1 - \phi_s$) from the gas-phase equations. This manipulation is responsible for the appearance of terms $1/(1-\phi_s)$ and ρ_g/ρ_s in the source term vector $\boldsymbol{S}$ [Eq. (3)]. The solid-phase volume fraction (ϕ_s) and the gas- and solid-phase density ratio (ρ_g/ρ_s) are generally small and could be neglected, but such an assumption does not introduce any significant simplification into the governing system of equations.

As one can easily notice, in the system of Eqs. (1–3) we do not include momentum or heat losses to the channel walls. Many works (see, e.g., Veyssiére and Khasainov[18]) show that these losses have a significant influence on the propagation of the detonation waves. In our case they would mask the behavior of a combustion model, and it would be very difficult to understand its properties and limitations. Thus, in this paper we will concentrate on ideal detonation waves and assume that the diameter of a computational shock and detonation tube is large and that all of the losses to the walls are negligibly small. Once the combustion model is tested and validated, then the losses can be included in the governing system of equations and the nonideal detonations can be studied numerically.

The governing system of equations is solved by using a time-splitting technique. The homogeneous part of the gas-phase equations is integrated by using the Harten–Yee flux-modified total-variation-diminishing (TVD) method (see, e.g., Hirsch[22]). For the condensed phase we apply a Godunov-type MUSCL Hancock TVD method (see Ref. 23) with special Riemann-problem solvers (see Ref. 24). The right-hand sides are integrated by using a fourth-order Runge–Kutta ordinary differential equation solver.

Combustion Model

The interphase mass transfer Δc is a simple mass flux from one phase to the other, which can be an effect of evaporation, condensation, and heterogeneous chemical reactions. The observations of burning aluminum particles reveal that combustion occurs mainly in the gas phase and that the burning zone is quite far from the particle surface (see, e.g., Wolfhard,[25] Bucher et al.,[26] and Wilson and Williams[27]). The burning rate is limited by diffusion of aluminum vapor and oxygen to the burning zone and combustion products in the opposite direction. Such a process is generally governed by a d^n-type law (see, e.g., Friedman and Macek,[28] Brooks and Beckstead,[29] and Liang and Beckstead[30]). In the case of aluminum, experimentally obtained values of the exponent n vary between 1.5 and 2. This uncertainty might be caused by the condensation of aluminum oxide on the burning droplet, which reduces the active surface of the particle. The oxide protects the particle from further penetration of oxygen and oxidation. It is also responsible for high scatter of aluminum-ignition temperatures published in the literature. In addition, aluminum and aluminum oxide change their state of condensation (melt, evaporate). At high temperatures, aluminum oxide starts to decompose into aluminum monoxide and oxygen, which stabilizes the temperature at a decomposition (or limiting) temperature (see, e.g., Glassman[31] and Borisov et al.[4]). These effects are sources of certain difficulties in the theoretical modeling of aluminum combustion.

For the purpose of our computations, we apply a modified version of an aluminum combustion model developed by Khasainov and Veyssiére.[15] The interphase mass exchange factor Δc has the following form:

$$\Delta c = (3\phi_s\rho_s/\tau)\left(1 + 0.276\sqrt{Re}\right) \qquad \text{for} \qquad T_s \geq T_{\text{ign}} \tag{11}$$

where Re is a relative Reynolds number based on the particle diameter and velocity difference between the two phases and τ is a characteristic time of combustion described by a d^2 -law:

$$\tau = K_r d_0^2 \tag{12}$$

K_r is a burning rate constant, and d_0 is an initial diameter of particles. This law is very simple, but computations conducted by Khasainov and Veyssiére[15] Veyssiére and Khasainov,[17,18] and Borisov et al.[4] were very successful. In Eq. (11) we simply assume that the mass transfer rate is proportional to the amount of aluminum present in the mixture and that it is some mean rate. This approach comes from the fact that it is very difficult to measure the size of burning aluminum particles because they are not very visible from their flame. This is especially true when micron-size particles are considered.

Although we will refer to Eqs. (11) and (12) as "the aluminum combustion model," it is in reality the aluminum evaporation model. In this research we assume that these equations are valid independently of the possible reaction mechanism and that they describe the solid- and liquid-aluminum consumption (evaporation) rate. The species (partial) interphase mass transfer factors are then defined as

$$\Delta c_k = \begin{cases} \Delta c & \text{for} \quad k = \text{Al} \\ 0 & \text{for} \quad k \neq \text{Al} \end{cases} \tag{13}$$

The evaporation starts when the particle temperature exceeds T_{ign}. We will refer to the parameter T_{ign} as "the ignition temperature," but we should remember that from the formal point of view, the definition of the ignition temperature is different. The ignition temperature is the temperature at which the energy release due to chemical reactions exceeds the energy loss through the convection, conduction, and radiation, and the reactions produce more energy than is removed from the system. This leads to an increase in the temperature of the system and is observed as an ignition. In our model, T_{ign} is the temperature at which the evaporation and combustion begin, and it can be referred to a process different from the actual ignition phenomena (e.g., to the onset to the gaseous mode of combustion).

Unlike the original version of the model developed by Khasainov and Veyssiére,[15] we do not utilize a heat of combustion, but assume that the heat release should be a direct effect of the applied combustion model. In our approach the chemical reactions can involve oxygen (O_2), aluminum vapor (Al), aluminum monoxide (AlO), and aluminum oxide (Al_2O_3). Although the latter generally does not exist in the gas phase, it is assumed that it can be present in the form of very fine particles that behave as a gas, and are treated as a gaseous component. The gaseous Al can be burnt, depending on the gas-phase properties, into Al_2O_3 or AlO, of course if there is sufficient amount of oxygen to burn with. For fuel-lean mixtures all aluminum vapor will be quickly oxidized and will not appear among combustion products. For fuel-rich mixtures the amount of oxygen can be insufficient to consume all aluminum vapor, and gaseous Al can appear in the mixture. If the gas-phase temperature T_g is lower than the decomposition temperature T_{dec} then the combustion product is aluminum oxide according to an exothermic reaction:

$$\text{Al} + \tfrac{3}{4}\text{O}_2 \Rightarrow \tfrac{1}{2}\text{Al}_2\text{O}_3 - 810.3 \times 10^3 \text{ J/mol} \qquad \text{for} \qquad T_g \le T_{\text{dec}} \tag{14}$$

At temperatures higher than the decomposition temperature, aluminum is burned into aluminum monoxide according to an endothermic reaction:

$$\text{Al} + \tfrac{1}{2}\text{O}_2 \Rightarrow \text{AlO} + 66.9 \times 10^3 \text{ J/mol} \qquad \text{for} \qquad T_g > T_{\text{dec}} \tag{15}$$

These reactions are infinitely fast, whereas the energetic effect is related to the number of moles of aluminum (Al). This method will stabilize the gas-phase temperature at some level close to the decomposition temperature. When the exothermic reaction equation (14) increases the temperature above the decomposition temperature, the endothermic reaction equation (15) tends to lower it back below the limiting value. Thus we limit the heat release by switching between two combustion reactions (products).

Base Case

In the following sections we will analyze the model described earlier. We will discuss the influence of various factors on the computed results, with special attention devoted to the combustion model and parameters describing its characteristics. Finally, we will compare our results with those of other theoretical models and experimental observations.

To facilitate our analyses, we have decided to select (arbitrarily) one case as a base for further comparisons. Thus, while changing one of free parameters of the system (T_{ign}, K_r, T_{dec}, d_0, and c_s), we can observe its impact on the system under consideration and obtained results.

The base case is a detonation wave propagating in a dilute mixture of 5-μm aluminum particles uniformly dispersed in an atmosphere of pure oxygen. An initial dust concentration is equal to $c_s = \rho_s\phi_s = 0.5$ kg/m^3. The ignition temperature is set to $T_{\text{ign}} = 1350$ K, the decomposition temperature is equal to $T_{\text{dec}} = 3500$ K, and the burning rate constant is $K_r = 4 \times 10^6$ s/m^2. These values have been chosen arbitrarily based on previous works of Khasainov and Veyssiére,[15] Veyssiére and Khasainov,[17,18] and Borisov et al.[4]

The computations are conducted on a uniformly spaced grid. The grid (cell) size is equal to 2 mm, and the detonation wave can propagate for 20 ms. Thus, the length of the computational domain is determined by a distance covered by the combustion wave. The right boundary condition is nonreflecting, whereas the left boundary is reflecting and emulates symmetry conditions. The detonation is initiated by means of a strong shock wave. Initial conditions for this and other cases presented in this paper are summarized in Table 1. In all of the computations, we assume that particles do not break up or agglomerate ($f = 0$).

Figure 1 presents a time evolution of a pressure distribution along the computational domain for time instants from 0 to 20 ms. A time delay between each curve is equal to 2 ms. After a short transition period, the detonation wave develops and steadily propagates in the channel. The detonation wave velocity is equal to

Table 1 Initial conditions for computations of an initiation and propagation of the detonation in aluminum dust–oxygen mixtures

Parameter	High-pressure part	Low-pressure part
Pressure	$p_g = 100$ bar	$p_g = 1$ bar
Gas-phase temperature	$T_g = 2000$ K	$T_g = 300$ K
Gas-phase velocity	$u_g = 0$ m/s	$u_g = 0$ m/s
Gas-phase composition	$Y_{\text{O}_2} = 1.00$	$Y_{\text{O}_2} = 1.00$
(mass fractions)	$Y_{\text{Al}} = 0.00$	$Y_{\text{Al}} = 0.00$
	$Y_{\text{AlO}} = 0.00$	$Y_{\text{AlO}} = 0.00$
	$Y_{\text{Al}_2\text{O}_3} = 0.00$	$Y_{\text{Al}_2\text{O}_3} = 0.00$
Solid-phase temperature	$T_s = 2000$ K	$T_s = 300$ K
Solid-phase velocity	$u_s = 0$ m/s	$u_s = 0$ m/s

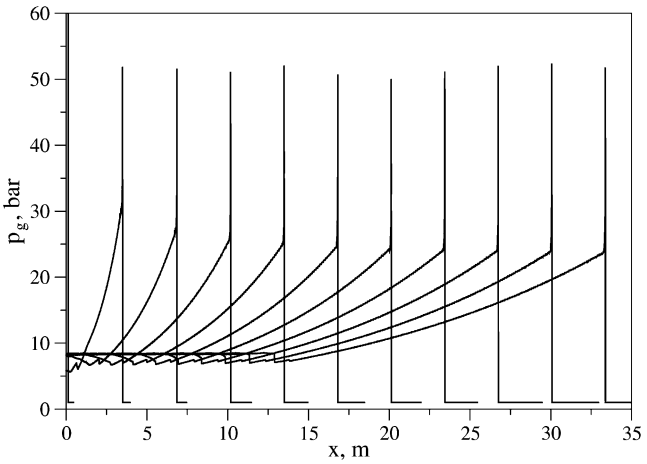

Fig. 1 Example time evolution of the detonation front (pressure profile) at $t = 0, 2, \ldots, 20$ ms.

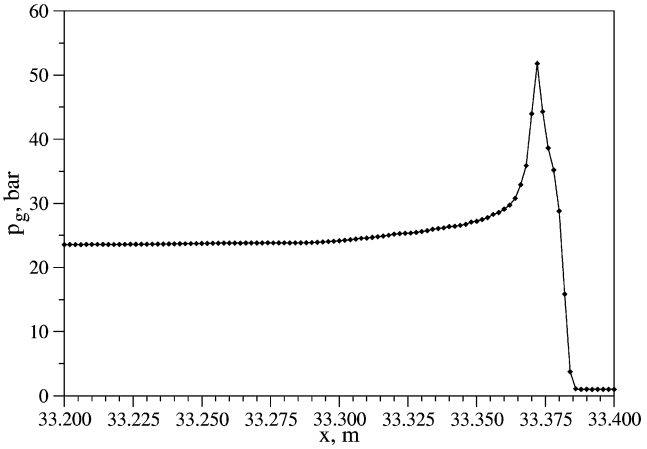

Fig. 2 Pressure profile in the detonation front at $t = 20$ ms (base case).

$D \approx 1656.9$ m/s, and the Chapman–Jouguet (C-J) detonation pressure is equal to $p_{\text{CJ}} \approx 22.9$ bar. The C-J pressure is "measured" at the point where a local gas-phase flow relative to the detonation front is sonic ($Ma = 1$). In the base case it is located about 71.4 cm behind the detonation front. The peak pressure (von Neumann spike) is equal to $p_{\text{vN}} \approx 51.8$ bar, but we should remember that this value strongly depends on a grid resolution.

Figures 2–7 show profiles of various parameters in the detonation front. Although the grid is relatively coarse, we can indicate a few interesting features. First, we can notice that the detonation front is relatively thick. In Figs. 3 and 4 we observe a significant temperature and velocity lags between the gas and solid phases. These figures indicate that even small particles have some inertia and that their acceleration and heating are distributed in space and time. The gas-phase temperature stabilizes close to the decomposition temperature, whereas the temperature of the condensed phase is slightly lower. We conclude that aluminum droplets have reached their boiling temperature.

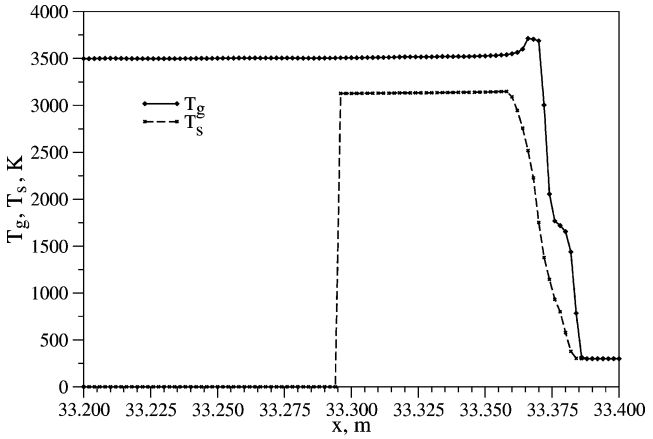

Fig. 3 Gas- and solid-phase temperature profiles in the detonation front at $t = 20$ ms (base case).

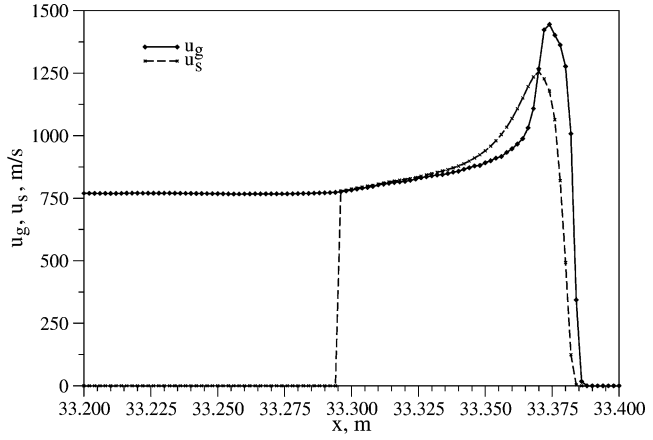

Fig. 4 Gas- and solid-phase velocity profiles in the detonation front at $t = 20$ ms (base case).

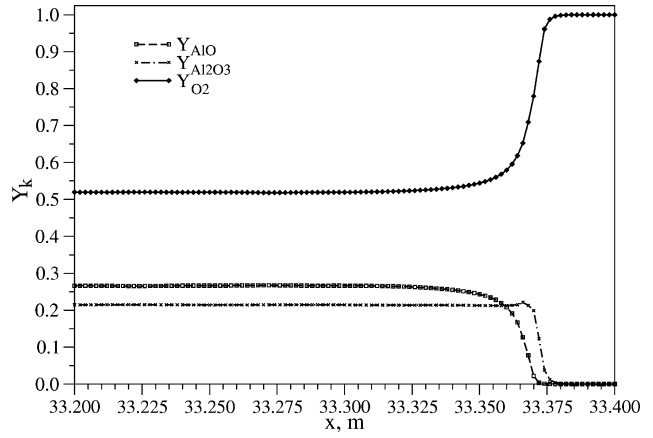

Fig. 5 Species distribution profiles in the detonation front at $t = 20$ ms (base case).

We also observe two kinks in the gas-phase temperature profiles. The first one, at about 1600–1750 K, is associated with the change of the state of condensation of solid aluminum. At $T_s \approx 933$ K, aluminum melts and this process consumes a significant amount of energy obtained from the gas phase. This leads to slower growth of the gas-phase temperature. The second kink is located close to the peak of the gas-phase temperature. The gas exceeds the decomposition temperature, which results in the change of the chemical reaction and combustion products. The latter is confirmed in Fig. 5: aluminum oxide is produced first behind the detonation front, whereas aluminum monoxide appears with some delay. Gaseous aluminum is not present in the system because the amount of oxygen is sufficient to consume all fuel.

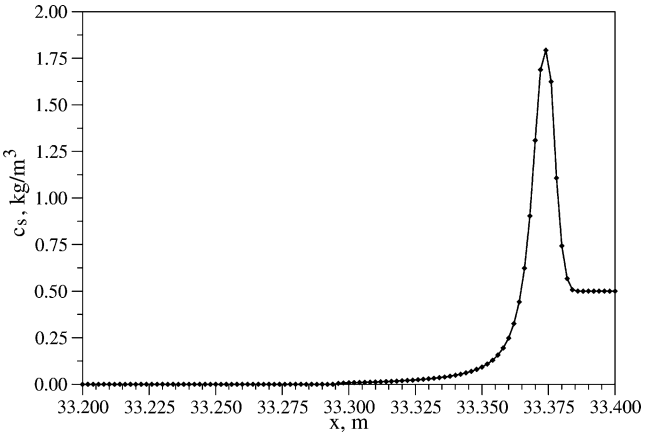

Fig. 6 Solid-phase concentration profile in the detonation front at $t = 20$ ms (base case).

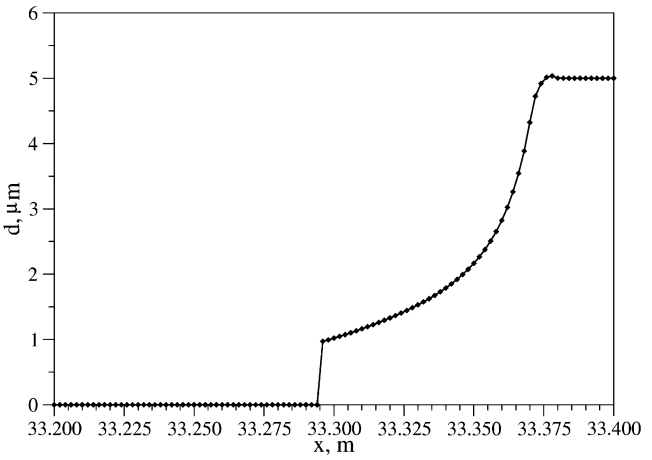

Fig. 7 Particle diameter profile in the detonation front at $t = 20$ ms (base case).

Another interesting feature is seen in Fig. 6. The propagating detonation wave pushes the condensed phase, which creates a high-concentration wave traveling just behind the detonation front. Thus the solid-phase concentration (in kilograms per cubic meter) just behind the detonation front can be a few times higher than in an undisturbed mixture ahead of the detonation wave. We should remember that the gas density behind the detonation front is also higher than in the undisturbed mixture and that the fuel/air ratio may have a profile different from the one shown in Fig. 6.

Finally we can notice that aluminum evaporates quickly. The gas-solid (-liquid) interaction (reaction) zone behind the detonation front is about 9.8 cm long (see, e.g., Fig. 3), which is almost one order of magnitude shorter than the distance to the C-J plane. A sudden drop of the solid-phase parameters visible in Figs. 3, 4, and 7 indicates that all solid and liquid aluminum have evaporated and that the mixture consists only of the gas phase.

Influence of the Combustion Model

A correct description of combustion is crucial to the proper modeling of the detonation process. The complexity of aluminum combustion does not allow us to apply a full kinetic model of aluminum oxidation as it involves heterogeneous and homogeneous chemical reactions, aluminum evaporation, diffusion of various species, etc. For practical reasons we have decided to apply a simplified aluminum combustion (evaporation) model that depends on three parameters: the ignition temperature T_{ign}, the burning rate constant K_r, and the decomposition temperature T_{dec}. In the following subsections we will show their influence on the computed results.

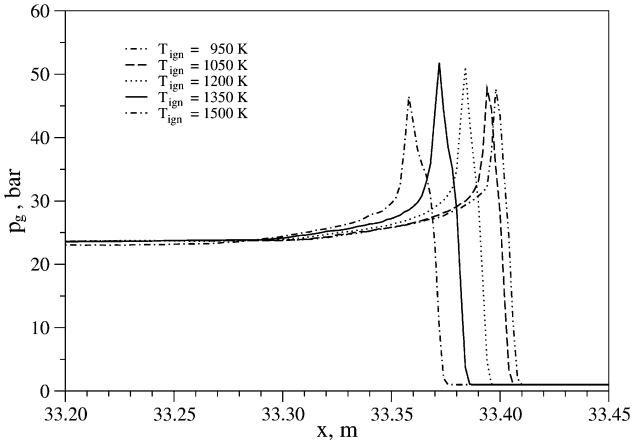

Fig. 8 Pressure profiles for various ignition temperatures at $t = 20$ ms.

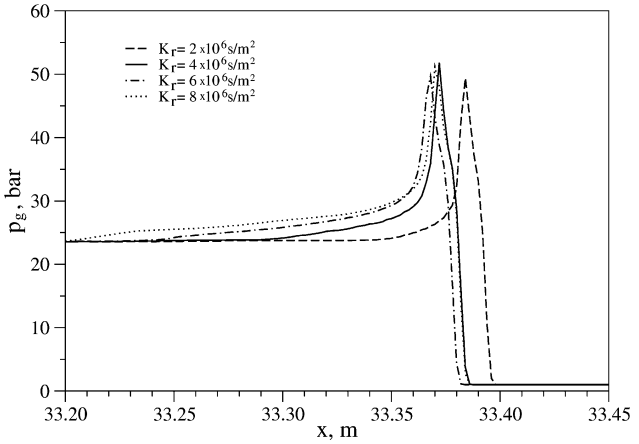

Fig. 9 Pressure profiles for various burning rates at $t = 20$ ms.

Ignition Temperature

Aluminum ignition is a complex process that involves heat transfer between the particle and the surrounding gas as well as heterogeneous reactions on the particle surface. Comparison of works of Friedman and Macek,[28] Price,[32] and Breiter et al.[33] indicates that the ignition temperature of aluminum particles can vary from about 750 to about 2350 K.

Figure 8 shows the influence of the ignition temperature on the computed profiles of the detonation wave. We consider five values of the ignition temperature: $T_{\text{ign}} = 950$ K (dashed–double dotted line), 1050 K (dashed line), 1200 K (dotted line), 1350 K (solid line), and 1500 K (dashed–dotted line). All other parameters are the same as in the base case. The positions of the detonation waves are in all of the cases almost identical. The detonation wave velocity decreases from $D \approx 1657.5$ to 1656.5 m/s (≈1-m/s change) as the ignition temperature increases from 950 to 1500 K. The peak (von Neumann) pressure varies from $p_{\text{vN}} \approx 46.5$ to 51.8 bar, while the C-J detonation pressure is in the range of 22.9–23.9 bar. The thickness of the detonation front near the von Neumann spike slightly increases with the increase of the ignition temperature, because aluminum needs more heat and time to reach higher ignition temperatures.

From Fig. 8, we can conclude that the choice of the ignition temperature has in practice no influence on the propagation of the detonation waves but it has influence on their development. If the ignition temperature is too high, then the solid phase is not able to reach the ignition point and the detonation cannot develop. For example, similar computations with $T_{\text{ign}} = 1750$ K do not lead to the development of the detonation wave.

Burning Rate

A very comparable conclusion comes from the analysis of the influence of the burning rate constant K_r on the detonation wave velocity and peak pressure. Figure 9 shows the detonation front profiles for $K_r = 2 \times 10^6$ s/m^2 (dashed line), 4×10^6 s/m^2 (solid line), 6×10^6 s/m^2 (dashed–dotted line), and 8×10^6 s/m^2 (dotted line). All other parameters are the same as in the base case. The differences in the position of the detonation fronts are in practice negligible, and the computations are insensitive to small variations (inaccuracy) of the burning rate constant.

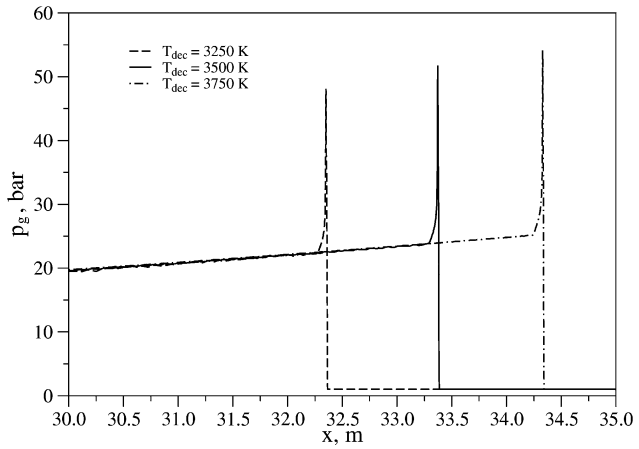

Fig. 10 Pressure profiles for various decomposition temperatures at $t = 20$ ms.

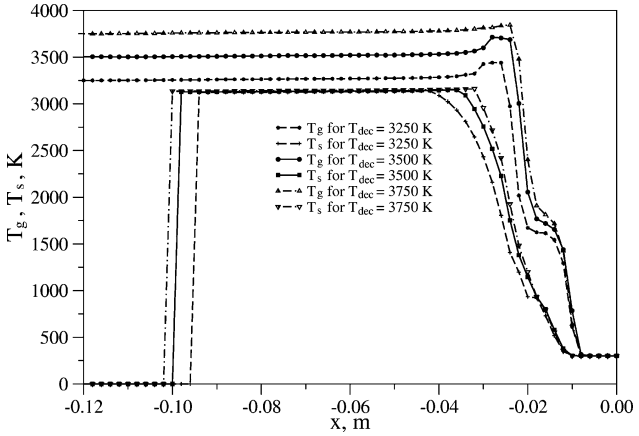

Fig. 11 Gas- and solid-phase temperature profiles for various decomposition temperatures at $t = 20$ ms.

Decomposition Temperature

The aluminum oxide decomposition reaction is not very well understood. In the literature, we can find at least three values of the temperature at which Al_2O_3 decomposes into AlO and O (or O_2). For example, Borisov et al.[4] quoted 3250 and 3800 K as the aluminum oxide decomposition temperature, whereas Liang and Beckstead[30] and Glassman[31] proposed about 4000 K.

Figures 10–15 show profiles of various parameters across the detonation fronts for the decomposition temperatures equal to $T_{\text{dec}} = 3250$ K (dashed lines), 3500 K (solid lines), and 3750 K (dashed–dotted lines). All other parameters are the same as in the base case. Figure 10 shows real positions of the detonation fronts as they have been obtained in our simulations, whereas in Figs. 11–15 all profiles have been repositioned so that all of the detonation waves begin at the same point. This manipulation should facilitate further comparisons.

The results show that the solution is very sensitive to the choice of the decomposition temperature. An increase of the decomposition temperature leads to faster and slightly stronger detonation waves by means of higher von Neumann spikes and C-J pressures. The detonation wave velocity increases from $D \approx 1604.1$ m/s for $T_{\text{dec}} = 3250$ K to $D \approx 1706.3$ m/s for $T_{\text{dec}} = 3750$ K. At the same time, the pressure at the von Neumann spike increases from $p_{\text{vN}} \approx 48.1$ to 54.2 bar, and the C-J pressure changes from $p_{\text{CJ}} \approx 21.4$ to 24.4 bar.

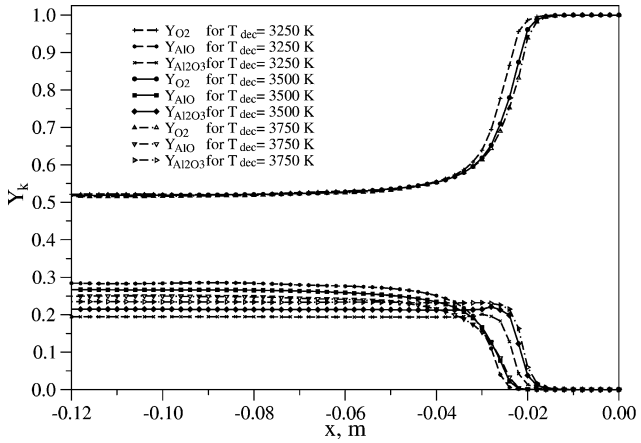

Fig. 12 Species mass fraction profiles for various decomposition temperatures at $t = 20$ ms.

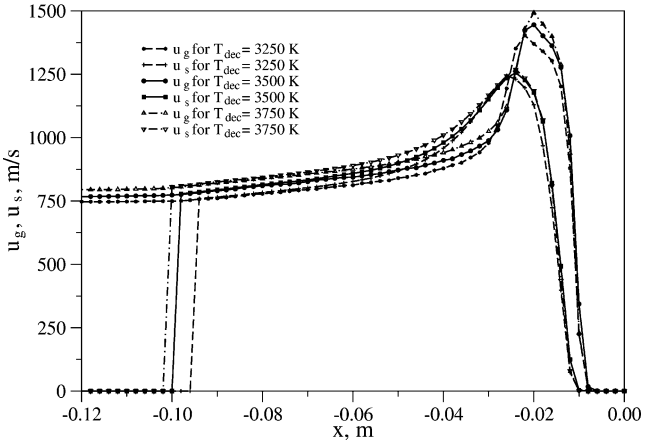

Fig. 13 Gas- and solid-phase velocity profiles for various decomposition temperatures at $t = 20$ ms.

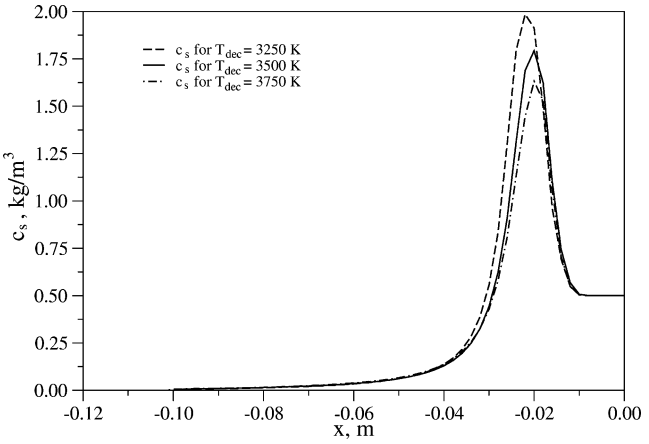

Fig. 14 Solid-phase concentration profiles for various decomposition temperatures at $t = 20$ ms.

In the combustion model applied in our simulations, the net energetic effect is governed by the competition between the exothermic and endothermic chemical reactions [see Eqs. (14) and (15)]. The increase of the decomposition temperature leads not only to higher temperatures behind the detonation wave (Fig. 11), but also to the increase of the mass fraction of aluminum oxide in the combustion products ($Y_{Al_2O_3}$ profiles in Fig. 12). Simply speaking, for higher decomposition temperatures more aluminum is burned into aluminum oxide Al_2O_3, and more energy is released in the system. The amount of aluminum monoxide AlO decreases (Fig. 12), because it is produced at temperatures higher than the decomposition temperature. If the system exceeds T_{dec}, then the main combustion product is AlO. This leads to the decrease of the temperature. If it drops below T_{dec}, then Al_2O_3 again becomes the main combustion product and the temperature can grow again. The increase of T_{dec} from 3250 to 3750 K significantly postpones the time instant when the endothermic reaction Eq. (15) is turned on, and this is responsible for the decrease of aluminum monoxide production. Finally, it also results in higher detonation wave velocities.

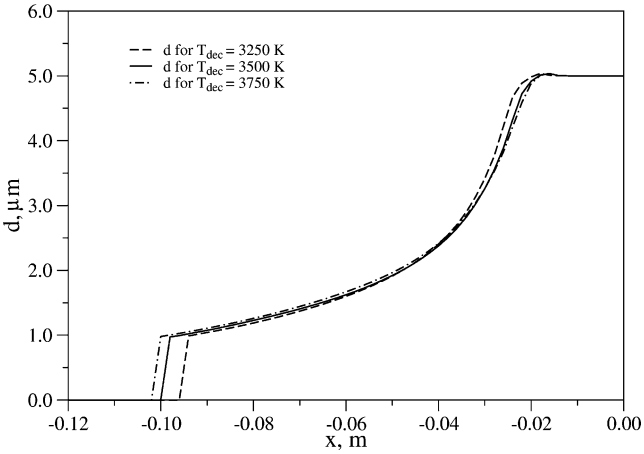

Fig. 15 Particle diameter profiles for various decomposition temperatures at $t = 20$ ms.

The gas-phase temperature behind the detonation front quickly stabilizes at the level close to the decomposition temperature (Fig. 11). The maximum solid-phase temperature is very similar in all of the cases (from 3136 to 3161 K). It is much higher than the aluminum boiling temperature at atmospheric conditions (≈2791 K), because the pressure behind the detonation front is quite high (over 20 bar), and aluminum boils at higher temperatures. In Fig. 11 we can also notice a kink of the solid-phase temperature associated with melting of solid aluminum. It is clearly visible only for $T_{dec} = 3250$ K, because of a slightly smaller temperature difference and heat flux between the gas and particles than for higher decomposition temperatures.

Another interesting feature comes from the comparison of Figs. 13–15. Although the velocity profiles (Fig. 13) are quite similar in all of the cases, the length of the reaction zone slightly increases and the maximum solid-phase concentration decreases (Fig. 14) with the increase of the decomposition temperature. Because the particle consumption rates are the same for all of the decomposition temperatures considered in this section (see, e.g., Fig. 15), the change of the reaction-zone length can be attributed to the dynamics of the flow phenomena. The increase of the detonation wave velocity leads to slightly different velocity lags between both phases. These differences accumulate, and for faster detonation waves they result in more stretched (smeared) reaction zones. This effect is only partially compensated by faster ignition and heating of the condensed phase.

Finally, we can conclude that the decomposition temperature can be used to fix the heat release and to adjust the computed solution to results obtained from other detonation models. Figure 16 shows the dependence of the detonation wave velocity on the decomposition temperature. Points indicate the computed results, and the dashed line is their linear approximation. It is clearly visible that such dependence can be used to match the one-dimensional simulations to the results obtained from e.g., the C-J detonation model.

Influence of the Particle Diameter

Another important factor that can have influence on the computed solution is an initial diameter of particles. Even though the initial particle diameter d_0 appears in the equation for the characteristic time of combustion described by Eq. (12), it is not a characteristic parameter of the combustion model. It is a property of the condensed

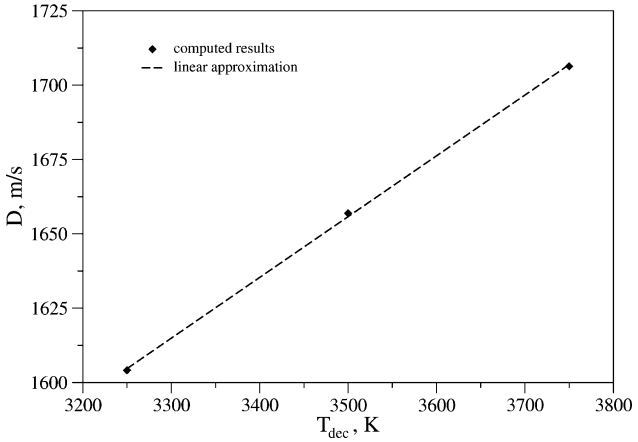

Fig. 16 Dependence of the detonation wave velocity on the decomposition temperature.

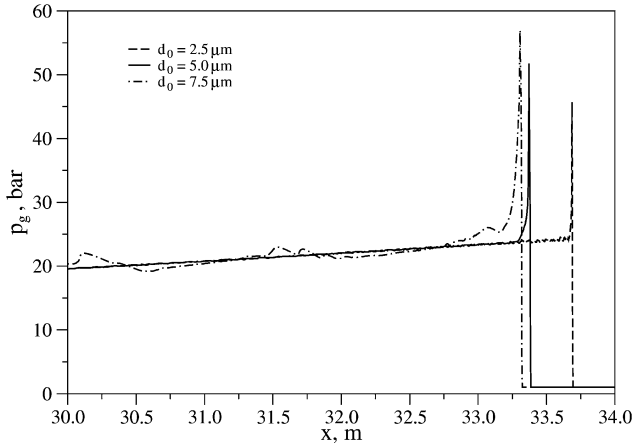

Fig. 17 Pressure profiles for various initial particle diameters at $t = 20$ ms.

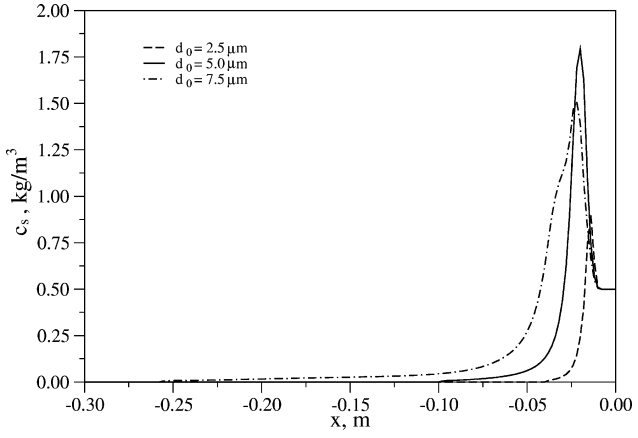

Fig. 18 Solid-phase concentration profiles for various initial particle diameters at $t = 20$ ms.

fuel and should be treated in a way slightly different from all previously considered factors.

According to the C-J detonation model, which is a model of an ideal detonation, the basic characteristics of the detonation depend only on the total heat release in the system. Thus, the detonation wave velocity and the C-J detonation pressure should be the same independently of the initial diameter of particles. In this section we will check whether the combustion model described by Eqs. (14) and (15) has this property and whether there are any limitations in its application.

Figures 17–20 show pressure, solid-phase concentration, gas- and solid-phase temperature, and species mass fraction profiles

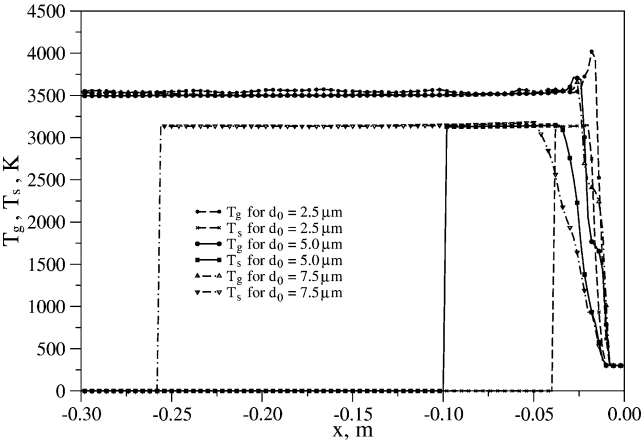

Fig. 19 Gas- and solid-phase temperature profiles for various initial particle diameters at $t = 20$ ms.

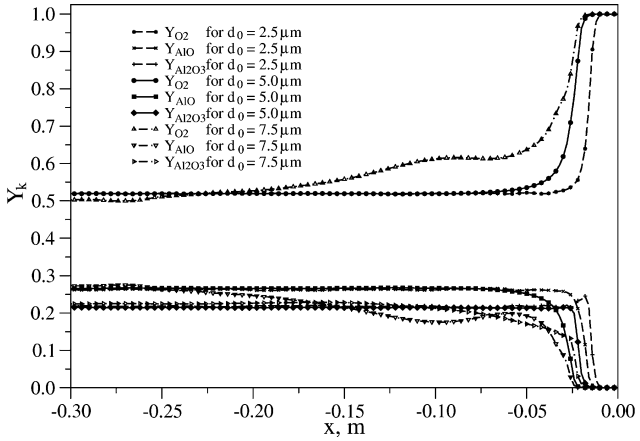

Fig. 20 Species mass fraction profiles for various initial particle diameters at $t = 20$ ms.

at $t = 20$ ms for three initial diameters of aluminum particles: $d_0 = 2.5$ μm (dashed lines), 5 μm (solid lines), and 7.5 μm (dashed–dotted lines). All other parameters are the same as in the base case. Similarly as in the preceding section, Fig. 17 shows real positions of the detonation fronts as they have been obtained in our simulations, whereas in Figs. 18–20 all profiles have been repositioned so that all of the detonation waves begin at the same point. In Figs. 19 and 20 we present only every second point on each profile, which should ease an analysis of these graphs.

The detonation wave velocity for 2.5-μm particles is equal to $D \approx 1667.6$ m/s, whereas for 5- and 7.5-μm particles it is almost the same and equal to 1656.9 and 1656.5 m/s, respectively. The C-J detonation pressure varies in the range from $p_{CJ} \approx 22.9$ to 25.5 bar, and the peak (von Neumann) pressures increase from $p_{vN} \approx 45.7$ to 57 bar with the increase of the initial particle diameter. We also observe strong pressure oscillations for the 7.5-μm particles that are visible in Fig. 17 (dashed–dotted line) as a nonmonotonic pressure drop far behind the detonation front. In this case, the peak pressure varies in the range from $p_{vN} \approx 40$ to 75 bar, which suggests that the detonation cannot propagate when the particles are larger than 8–10 μm. Our simulations with 10- and 15-μm particles failed, because it was not possible to initiate a steady detonation in such mixtures. Large particles have high mechanical and thermal inertia, and the heat transferred from the gas to the particles just behind the shock-wave front is insufficient to increase the particle temperature to the ignition point. A very similar conclusion has been presented by Borisov et al.,[4] who were not able to detonate such mixtures even by using very strong initiators.

Figure 18 shows that the solid-phase concentration behind the detonation front grows with the increase of the initial particle diameter, although the initial dust concentration ahead of the detonation

wave is the same. It may seem that the case of 7.5-μm particles is an exception here, but we should remember the pressure oscillations obtained for this case. A comparison of the solid-phase concentration profiles for various time instants reveals that its maximum can vary in the range from 1.5 to 3 kg/m^3. These oscillations are related to the galloping mode of propagation observed in this simulation. This behavior of the computed detonation waves becomes more visible for particles larger than about 5.5–6 μm. It is caused by differences in the burning rate, drag force coefficient, and heat transfer from the gas to the particles. These factors strongly depend on the particle diameter. Small particles are quickly accelerated, heated, ignited, and burnt, and the solid-phase concentration behind the detonation wave quickly decreases. Larger particles need more time and energy to reach the ignition temperature. Their ignition leads to a small local explosion, which pushes the detonation wave forward. The latter starts to heat another portion of the fuel, which again needs some time to reach the ignition temperature. This process is periodic and can be observed as small "jumps" of the detonation wave and as the galloping mode of its propagation.

We notice here that the threefold increase of the initial diameter of particles results in a change of the detonation wave velocity smaller than 0.7%. The differences in the position of the detonation waves seen in Fig. 17 arise from the accumulated differences in their development processes. Even though the length of the phase interaction (burning) zone significantly grows with the increase of the initial diameter of particles (see, e.g., solid-phase temperature profiles in Fig. 19) the particles reach very similar temperatures. The same effect is visible also in the case of the gas-phase temperatures far behind the detonation front. The main differences are located in the detonation front and are related to the time needed to heat, ignite, and consume the particles. Obviously, the smallest particles ignite and burn quickly and their combustion leads to slightly higher maximum temperatures (Fig. 19), but the final composition of the combustion products is in all of the cases very similar (Fig. 20). Because the mass proportions of the combustion products (mainly Al_2O_3 and AlO) define the total heat release, in all of the cases the energy produced in aluminum combustion is almost the same, and the detonation wave velocities are also very similar. Unfortunately, the C-J detonation model does not give us information about the structure of the detonation front, and it cannot be compared directly with the results obtained in our simulations.

To check the range of applicability of the combustion model described in this paper, we compare the detonation wave velocities (Fig. 21), and peak (von Neumann) and C-J pressures (Fig. 22) for initial particle diameters ranging from $d_0 = 0.5$ to 7.5 μm. Figure 21 clearly shows that for particles larger than 2.5–3 μm, the particle diameter has a minor influence on the detonation wave velocity, provided that they are sufficiently small to allow for the development of the detonation wave. For particles smaller than 2.5–3 μm, the model cannot be applied, because the detonation wave velocity

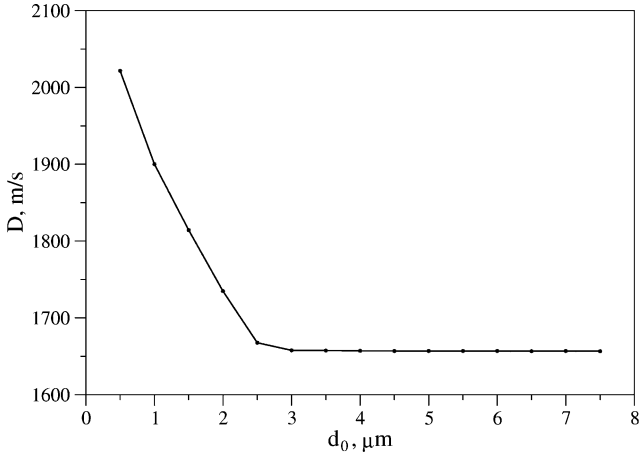

Fig. 21 Detonation wave velocity as a function of the initial particle diameter.

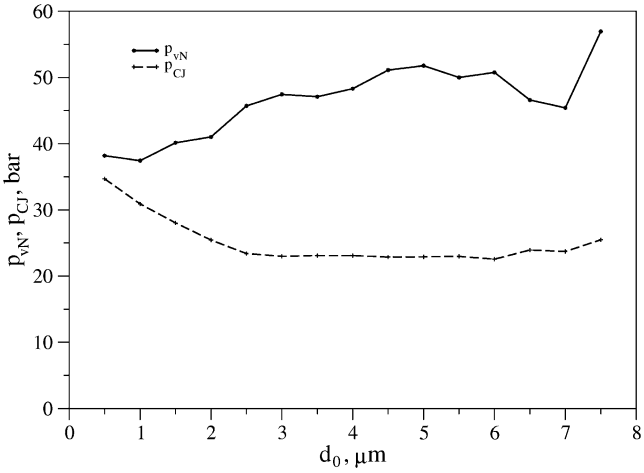

Fig. 22 Pressure at von Neumann spike and C-J pressure as functions of the initial particle diameter.

becomes a function of the initial particle diameter. Such behavior can be explained by the fact that the combustion always starts with the exothermic reaction equation (14), because the gas-phase temperature just after ignition is higher than T_{ign} and smaller than T_{dec}. The combustion product is then aluminum oxide, which leads to the growth of the temperature. The endothermic reaction equation (15) starts with some delay after the ignition. Very small particles are consumed quickly, and only a small portion of aluminum is burned into AlO, and the combustion wave cannot achieve an equilibrium. (Small differences in the detonation wave velocities discussed in the preceding paragraph can be also explained in this way, but the nonequilibrium is much smaller than in the case of very fine dust.) Thus, for very small particles, the net heat release is significantly higher than for larger particles, and we have to limit the applicability of the combustion model to particles larger than about 2.5–3 μm. For smaller particles, one should include an additional, highly endothermic aluminum oxide decomposition reaction of the form

$$Al_2O_3 \Rightarrow 2AlO + \tfrac{1}{2}O_2 + 1754.5 \times 10^3 \text{ J/mol} \qquad \text{for} \qquad T_g > T_{dec} \tag{16}$$

which should lead to the chemical equilibrium between all combustion products. Another possibility is to remove a temperature limitation imposed on Eq. (14) and to exchange Eqs. (15) and (16).

A similar conclusion comes from the analysis of the C-J pressures shown in Fig. 22 (dashed line). For particles in the range of 2.5–6 μm, we observe a very small variation of the C-J pressure with the change of the initial particle diameter. For particles larger than 6 μm, the effect of the galloping detonation influences the pressure profiles behind the detonation front, but the applicability of the C-J model to the galloping detonations should be considered with care, because such detonation is not a steady-state process. The effect of the galloping detonation is also visible in the dependence of peak pressures (solid line) on the initial particle diameter as a nonsmooth graph, especially for particles larger than 7 μm. Finally, we can limit the applicability of the combustion model to particle diameters in the range of 2.5–6 μm.

Influence of the Dust Concentration

One of the most interesting and important aspects for practical applications is the dependence of the detonation parameters (e.g., propagation velocity, C-J and von Neumann pressures) on fuel concentration. Such information, presented in a graphical form, directly indicates a real detonation hazard and detonability limits.

Figure 23 shows the dependence of the detonation wave velocity D and the C-J detonation wave velocity D_{CJ} on fuel concentration in an undisturbed mixture ahead of the detonation wave. Similar dependence of the peak (von Neumann) pressure p_{vN} and the C-J pressure p_{CJ} on the aluminum concentration is shown in Fig. 24. In

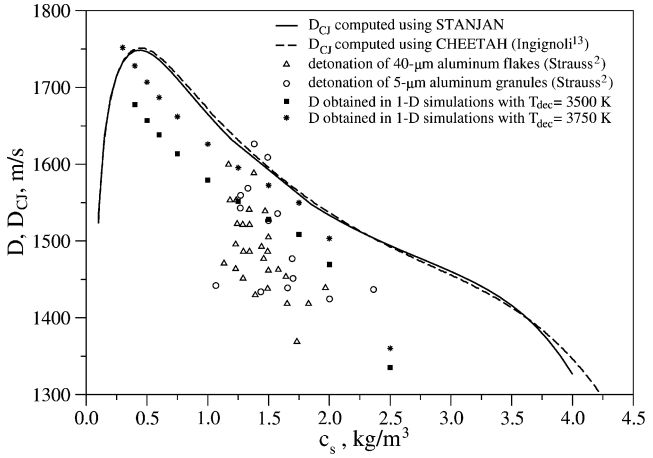

Fig. 23 Dependence of the detonation wave velocity D and the C-J detonation wave velocity D_{CJ} on the aluminum-dust concentration for aluminum–oxygen mixtures.

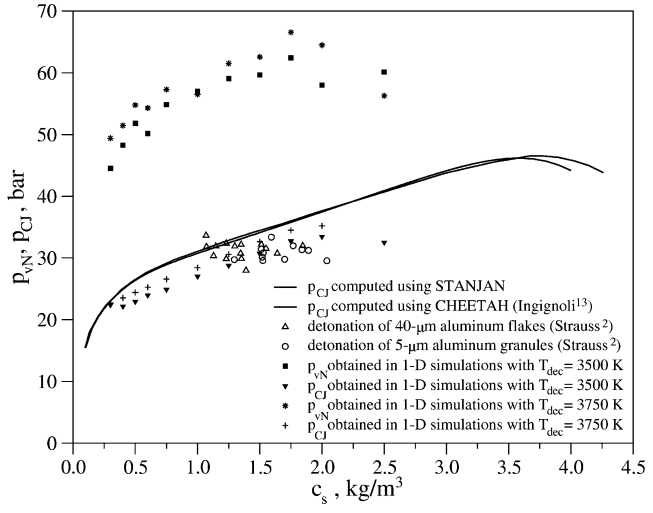

Fig. 24 Dependence of the detonation pressure p_{max} and the C-J detonation pressure p_{CJ} on the aluminum-dust concentration for aluminum–oxygen mixtures.

both figures we compare the computed results with other theoretical and experimental data. They are as follows:

1) The solid lines indicate results obtained from the C-J computations using STANJAN computer code. These results cover the range of concentrations from very lean ($c_s = 0.1$ kg/m^3) to very rich ($c_s = 4$ kg/m^3) mixtures. For aluminum dust–oxygen mixtures, the stoichiometric dust concentration is equal to $c_s \approx 1.452$ kg/m^3 (assuming aluminum monoxide Al_2O_3 as the combustion product), the corresponding C-J detonation wave velocity is $D_{CJ} \approx 1598$ m/s, and the C-J pressure is $p_{CJ} \approx 33.8$ bar. In these computations we assume that the undisturbed mixture contains oxygen O_2 and solid aluminum Al, whereas the combustion products can consist of condensed aluminum oxide Al_2O_3, aluminum vapor Al, aluminum oxides AlO, AlO_2, Al_2O, and Al_2O_2, atomic oxygen O, and molecular oxygen O_2.

2) The dashed lines are similar results obtained by Ingignoli[13] using CHEETAH computer code.

3) The △ and ⊙ indicate experimental data published by Strauss[2] for the detonation of 40-μm aluminum flakes and 5-μm aluminum granules in oxygen, respectively.

4) The ■ are the detonation wave velocities and peak (von Neumann) pressures obtained in our one-dimensional simulations for the initial solid-phase concentrations ranging from 0.3 to 2.5 kg/m^3. All other parameters are the same as in the base case. The ▼ in Fig. 24 indicate the C-J pressures that correspond to the peak pressures ■.

5) The $*$ are the detonation wave velocities and peak pressures obtained in similar computations as in the preceding but for the decomposition temperature set to $T_{dec} = 3750$ K. The + in Fig. 24 indicate the C-J pressures that correspond to the peak pressures $*$.

The results gathered in Fig. 23 show a qualitative agreement of our numerical simulations with the results of the C-J computations. The one-dimensional simulations reproduce the trend predicted by the C-J model, but the computed values of the detonation wave velocity and C-J pressure are lower than results obtained from the C-J detonation model. Significant differences are also visible for aluminum concentrations smaller than about 0.4 kg/m^3 and larger than about 2 kg/m^3, which set the applicability limits of the combustion model described in this paper.

The lower limit appears because there is not enough fuel that could be burned into aluminum monoxide and lead to the chemical equilibrium between all combustion products. Thus the reason is the same as in the case of very fine dust. Inclusion of Eq. (16) should lead to the equilibrium and can extend the applicability of the combustion model to initial dust concentrations lower than 0.4 kg/m^3.

The cause of the upper limit is more complex. At high concentration, the condensed phase has high thermal capacity and particles (droplets) work as a heat sink. The gas phase cools quickly behind the detonation front, which also results in a quick decrease of the pressure. The C-J plane then appears much closer to the detonation front than for lower aluminum concentrations. Thus, only part of the fuel evaporates before the C-J plane, and only part of the total accessible heat release can propel the detonation wave.

We have to point out that we introduce the upper applicability limit because we do not know how to interpret the results obtained for $c_s > 2$ kg/m^3. Obviously, the C-J detonation model cannot provide us any clue because of its simplicity. It considers only what is far ahead of the detonation wave and the C-J point and does not take into account what happens between them or the transient process that leads to the development of the detonation wave. Our uncertainty comes also from the fact that Ingignoli[13] has not encountered such problems.

Let us concentrate on the range of concentrations between the lower and upper applicability limits. The differences between the detonation parameters obtained from the C-J model and one-dimensional simulations can be attributed to various simplifications introduced in both models. Specifically, the combustion model used in our computations employs two infinitely fast chemical reactions (equilibrium combustion model) and is limited by the rate of aluminum evaporation. The C-J detonation model also employs an equilibrium chemistry but involves more species. In reality the combustion process can be much more complex and involve many chemical reactions with finite chemical kinetic rates. The results can obviously depend on some constants applied in the combustion model. As one can easily notice, the increase of the decomposition temperature from $T_{dec} = 3500$ to 3750 K leads to a better match of the one-dimensional and C-J computations. Analysis of Fig. 16 suggests that the one-dimensional simulations should match the results obtained from the C-J detonation model for the decomposition temperature in the range of 3900–3950 K.

The comparison of the computed results and experimental data suggests that they also agree quantitatively, but the latter present a significant scatter of the results. First, they cover a much narrower range of concentrations than we could consider in our computations. Although the computed detonation-wave velocities and their trend are within the values obtained by Strauss,[2] we cannot conclude that we have been able to reproduce his experiments. The peak pressures (von Neumann spikes) significantly exceed the experimental values, whereas the C-J pressures agree quite well with them. One should remember that pressure transducers used in experimental studies have finite time resolution and "measure" pressure closer to the C-J pressure than to the von Neumann spike. We should also remember that the C-J pressure is a mathematical solution of some system of equations (see also Lee[34]). The C-J model is generally unable to predict the peak pressure at the von Neumann spike without additional information about the chemical kinetics or the structure of the detonation front.

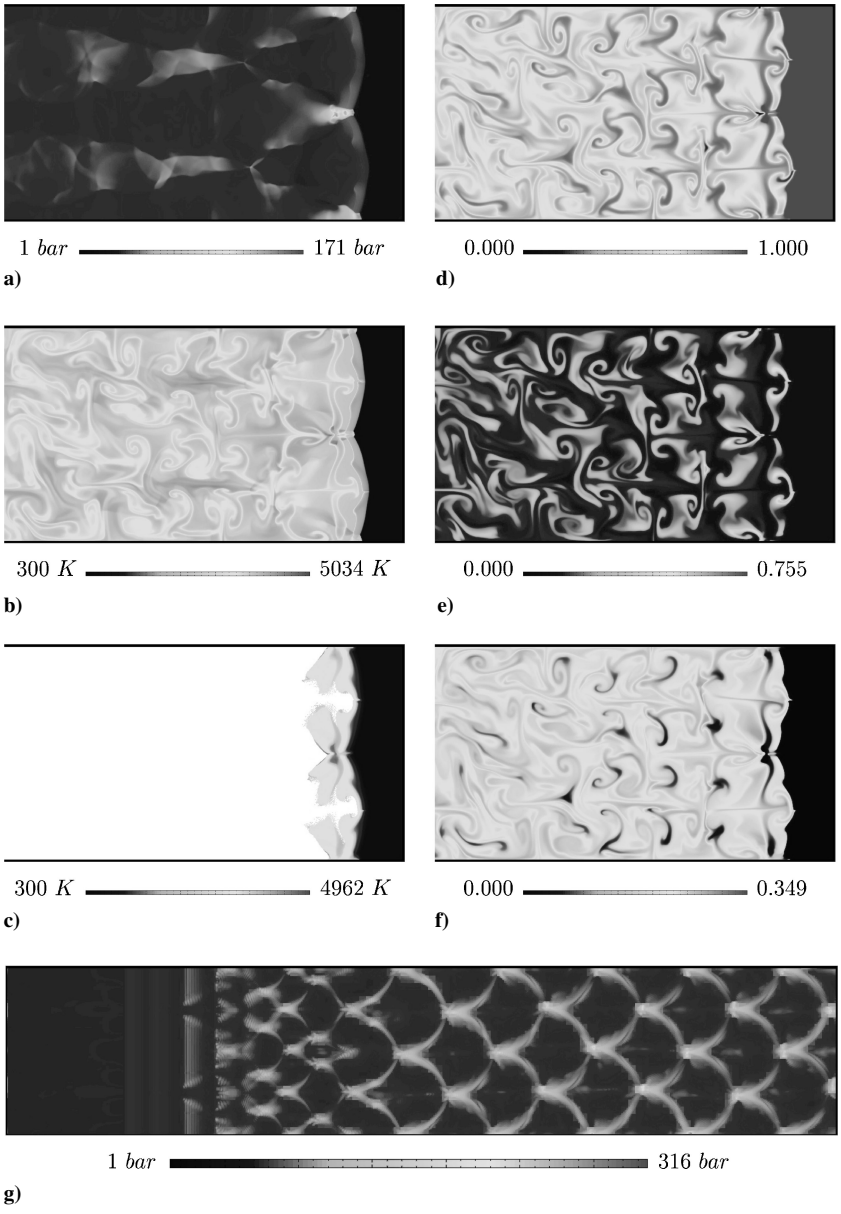

Fig. 25 Two-dimensional simulation of the detonation in the aluminum dust–oxygen mixture ($c_s = 0.3$ kg/m^3, $d_0 = 2.5$ μm, $T_{ign} = 1350$ K, $T_{dec} = 3750$ K, $K_r = 4 \times 10^6$ s/m^2): a) pressure, b) gas- and c) solid-phase temperature, d) oxygen, e) aluminum monoxide, and f) aluminum oxide mass fraction distributions at 520 μs, and g) traces of the maximum pressure.

Another source of differences is the absence of momentum and energy losses to the channel walls. In all experimental conditions, the size of test equipment is limited and the losses are not negligible. One should also remember that the detonation is a multidimensional dynamic process (see Fig. 25 for example results of two-dimensional simulations of the detonation with the earlier mentioned combustion model) and that the dust applied in the experiments is usually not uniform. It contains particles of very different sizes and shapes, and the mechanical and thermal interactions between the gas and solid phases in the detonation wave front can be very extended in space and time. Thus, the conditions encountered in real experiments can exceed the limitations of the C-J model, and, in opposition to the classical single-phase C-J model, the multiphase flow can be quite "far" from the assumptions imposed in the C-J theory. Additional uncertainty comes from the fact that Strauss[2] has used relatively short and small tubes (length 2.7 m, diameter 19.5–55.2 mm), whereas he has measured quite long induction distances. He probably has not been able to obtain a steady self-sustained detonation.

Conclusions

In this paper we presented results of one-dimensional parametric studies of the combustion model for numerical simulations of detonation waves propagating in aluminum dust–oxygen two-phase mixtures. The computational model used a simplified two-step aluminum-dust combustion model. The first step was the evaporation process described by the d^2-type law, and the second one was the aluminum-vapor oxidation. Depending on the gas-phase temperature, the combustion product was either aluminum oxide or aluminum monoxide. We analyzed the influence of various factors on the characteristic parameters of the detonation and compared the computed results with those of other models and experimental data.

The computations showed the qualitative agreement of the computed results with the Chapman-Jouguet (C-J) detonation model. The computed values of the detonation velocity also lie within the range of experimental results, but certain scatter of the experimental data does not allow for an unambiguous conclusion about their quantitative agreement. The parametric studies of aluminum dust–oxygen detonations showed that the initial solid-phase concentration and the combustion model have a major influence on the computed solutions. The initial particle diameter (with the exception of very fine dust) and the ignition temperature have a minor effect on the propagation of the detonation waves but are limiting factors for their development. In the case of large particles or very high ignition temperatures, the detonation cannot develop even if the initiator is

very strong. On the other hand, the decomposition temperature has a much stronger influence on the system, because it limits the energy release in the combustion process. It is a threshold value, which changes the combustion mechanism, and can be used to fix the heat release in the system. By the proper choice of the decomposition temperature (e.g., its increase to $T_{dec} \approx 3950$ K) we can reproduce the results obtained from the C-J detonation model, and such a calibrated model can be used also in two- and three-dimensional simulations.

The combustion model presented in this paper is not a perfect one, but it is a step toward kinetic modeling of aluminum-dust combustion and computer simulations of the detonation waves in multiphase mixtures. Its major advantages are simplicity and small computational cost, which are especially important in multidimensional simulations. Example results of the two-dimensional computations with an application of the combustion model described earlier are shown in Fig. 25. Figures 25a–25f cover a part of the domain (0.225×0.12 m), and Fig. 25g shows the whole computational domain (0.6×0.12 m). The traces of the maximum pressure (Fig. 25g) are equivalent to the smoke-foil records obtained from experimental studies. White in Fig. 25c presenting the solid-phase temperature indicates a lack of the condensed phase in the mixture. These pictures reveal the structure and mechanism of propagation of the detonation wave in heterogeneous mixtures. Thus, the combustion model shows its usefulness and efficiency in such studies, and after some improvements its application can be extended to a wide spectrum of initial conditions. This will be a future direction of our studies.

References

[1]Eckhoff, R., "Dust Explosions in the Process Industries," Butterworth–Heinemann, Oxford, 1997.

[2]Strauss, W. A., "Investigation of the Detonation of Aluminum Powder–Oxygen Mixtures," *AIAA Journal*, Vol. 6, No. 9, 1968, pp. 1753–1756.

[3]Tulis, A. J., and Selman, J. R., "Detonation Tube Studies of Aluminum Particles Dispersed in air," *Proceedings of the 19th Symposium (International) on Combustion*, Combustion Inst., Pittsburgh, PA, 1982, pp. 655–663.

[4]Borisov, A. A., Khasainov, B. A., Saneev, E. L., Fomin, I. B., Khomik, S. V., and Veyssiére, B., "On the Detonation of Aluminum Suspension in Air and in Oxygen," *Dynamic Structure of Detonation in Gaseous and Dispersed Media*, edited by A. A. Borisov, Kluwer Academic, 1991, pp. 215–253.

[5]Zhang, F., Grönig, H., and Van de Ven, A., "DDT and Detonation Waves in Dust–Air Mixtures," *Shock Waves*, Vol. 11, No. 1, 2001, pp. 53–71.

[6]Tulis, A. J., "On the Unconfined Detonation of Aluminum Powder–Air Clouds," *Proceedings of the First (International) Colloquium on Explosibility of Industrial Dusts*, Baranów, 1984, pp. 178–186.

[7]Tulis, A. J., and Selman, J. R., "Unconfined Aluminum Particle Two-Phase Detonation in Air," *Dynamics of Shock Waves, Explosions, and Detonations*, edited by J. R. Bowen, N. Manson, A. K. Oppenheim, and R. I. Soloukhin, Vol. 94, Progress in Astronautics and Aeronautics, AIAA, New York, 1985, pp. 277–292.

[8]Ingignoli, W., Veyssiére, B., and Khasainov, B. A., "Study of Detonation Initiation in Unconfined Aluminum Dust Clouds," *Gaseous and Heterogeneous Detonations, Science to Applications*, edited by G. Roy et al., 1999, pp. 337–350.

[9]Zhang, F., Thibault, P. A., and Murray, S. B., "Transition from Deflagration to Detonation in an End Multiphase Slug," *Combustion and Flame*, Vol. 114, No. 1–2, 1998, pp. 13–25.

[10]Veyssiére, B., "Double-Front Detonations in Gas–Solid Particles Mixtures," *Dynamics of Shock Waves, Explosions, and Detonations*, edited by J. R. Bowen, N. Manson, A. K. Oppenheim, and R. I. Soloukhin, Vol. 94, Progress in Astronautics and Aeronautics, AIAA, New York, 1985, pp. 264–276.

[11]Veyssiére, B., "Structure of the Detonation in Gaseous Mixtures Containing Aluminum Particles in Suspension," *Dynamics of Explosions*, edited by J. R. Bowen et al., Vol. 106, Progress in Astronautics and Aeronautics, AIAA, New York, 1986, pp. 522–544.

[12]Veyssiére, B., Bouriannes, R., and Manson, N., "Detonation Characteristics of Two Ethylene–Oxygen–Nitrogen Mixtures Containing Aluminum Particles in Suspension," *Gasdynamics of Detonations and Explosions*, edited by J. R. Bowen et al., Vol. 75, Progress in Astronautics and Aeronautics, AIAA, New York, 1981, pp. 423–438.

[13]Ingignoli, W., "Etude de la Formation et de la Propagation des Détonations dans des Suspensions de Particules d'Aluminium en Atmosphere Oxydante ou Réactive," Ph.D. Dissertation, Université Poitiers, Poitiers, France, 1999.

[14]Fedorov, A. V., Khmel', T. A., and Fomin, V. M., "Non-Equilibrium Model of Steady Detonations in Aluminum Particles–Oxygen Suspensions," *Shock Waves*, Vol. 9, No. 5, 1999, pp. 313–318.

[15]Khasainov, B. A., and Veyssiére, B., "Steady, Plane, Double-Front Detonations in Gaseous Detonable Mixtures Containing a Suspension of Aluminum Particles," *Dynamics of Explosions*, edited by A. L. Kuhl et al., Vol. 114, Progress in Astronautics and Aeronautics, AIAA, Washington, DC, 1988, pp. 284–299.

[16]Khasainov, B. A., and Veyssiére, B., "Initiation of Detonation Regimes in Hybrid Two-Phase Mixture," *Shock Waves*, Vol. 6, No. 1, 1996, pp. 9–15.

[17]Veyssiére, B., and Khasainov, B. A., "A Model for Steady, Plane, Double-Front Detonation (DFD) in Gaseous Explosive Mixtures with Aluminum Particles in Suspension," *Combustion and Flame*, Vol. 85, No. 1–2, 1991, pp. 241–253.

[18]Veyssiére, B., and Khasainov, B. A., "Structure and Multiplicity of Detonation Regimes in Heterogeneous Hybrid Mixtures," *Shock Waves*, Vol. 4, No. 4, 1995, pp. 171–186.

[19]Henderson, C. B., "Drag Coefficients of Spheres in Continuum and Rarefied Flows," *AIAA Journal*, Vol. 14, No. 6, 1976, pp. 707, 708.

[20]Carlson, D. J., and Hoglund, R. F., "Particle Drag and Heat Transfer in Rocket Nozzles," *AIAA Journal*, Vol. 2, No. 11, 1964, pp. 1980–1984.

[21]Kee, R. J., Warnatz, J., and Miller, J. A., "A FORTRAN Computer Code Package for the Evaluation of Gas-Phase Viscosities, Conductivities, and Diffusion Coefficients," Sandia National Labs., Rept. SAND80-83-8209, Livermore, CA, 1983.

[22]Hirsch, C., *Numerical Computation of Internal and External Flows*, Vol. 1–2, Wiley, New York, 1995.

[23]Toro, E. F., *Riemann Solvers and Numerical Methods for Fluid Dynamics*, Springer-Verlag, Heidelberg, Germany, 1997.

[24]Benkiewicz, K., and Hayashi, A. K., "Numerical Simulations of Initiation and Propagation of Detonation in Gas–Solid 2-Phase Mixtures," *Proceedings of the 14th Japanese Symposium on Computational Fluid Dynamics* [CD-ROM], Tokyo, 2000.

[25]Wolfhard, H. G., *Heterogeneous Combustion*, Vol. 15, Progress in Astronautics and Aeronautics, AIAA, New York, 1964.

[26]Bucher, P., Yetter, R. A., Dryer, F. L., Parr, T. P., Hanson-Parr, D. M., and Vicenzi, E. P., "Flame Structure Measurement of Single, Isolated Aluminum Particles Burning in Air," *Proceedings of the Twenty-Sixth Symposium (International) on Combustion*, Combustion Inst., Pittsburgh, PA, 1996, pp. 1899–1908.

[27]Wilson, R. P., and Williams, F. A., "Experimental Study of the Combustion of Single Aluminum Particles in O_2/Ar," *Proceedings of the Thirteenth Symposium (International) on Combustion*, Combustion Inst., Pittsburgh, PA, 1971, pp. 822–845.

[28]Friedman, R., and Macek, A., "Ignition and Combustion of Aluminum Particles in Hot Ambient Gases," *Combustion and Flame*, Vol. 6, 1962, pp. 9–19.

[29]Brooks, K. P., and Beckstead, M. W., "Dynamics of Aluminum Combustion," *Journal of Propulsion and Power*, Vol. 11, No. 4, 1995, pp. 769–780.

[30]Liang, Y., and Beckstead, M. W., "Numerical Simulation of Quasi-Steady, Single Aluminum Particle Combustion in Air," AIAA Paper 98-0254, 1998.

[31]Glassman, I., "Combustion of Metals Revisited—Thermodynamically," *Proceedings of the Eastern States Section of the Combustion Institute*, Princeton, NJ, 1993, pp. 17–26.

[32]Price, E. W., "Combustion of Metalized Propellants," *Fundamentals of Solid-Propellant Combustion*, edited by K. Kuo, Vol. 90, Progress in Astronautics and Aeronautics, AIAA, New York, 1984, pp. 479–513.

[33]Breiter, A. L., Mal'tsev, v. M., and Popov, E. I., "Models of Metal Ignition," *Fizika Goreniya i Vzryva*, Vol. 13, No. 4, 1976, pp. 558–570.

[34]Lee, J. H. S., "Dynamic Parameters of Gaseous Detonations," *Annual Review of Fluid Mechanics*, Vol. 16, 1984, pp. 311–336.

M. Sichel
Associate Editor